

Review

Perovskite Thin Films Solar Cells: The Gas Quenching Method

Maria Azhar, Yenal Yalcinkaya, Daniele T. Cuzzupè, Yekitwork Abebe Temitmie, Muhammad Irfan Haider and Lukas Schmidt-Mende *

Department of Physics, University of Konstanz, 78457 Konstanz, Germany

* Correspondence: lukas.schmidt-mende@uni-konstanz.de

How To Cite: Azhar, M.; Yalcinkaya, Y.; Cuzzupè, D.T.; et al. Perovskite Films Solar Cells: The Gas Quenching Method. *Materials and Sustainability* 2025, 1(1), 5. <https://doi.org/10.53941/matsus.2025.100005>.

Received: 18 November 2024

Revised: 6 January 2025

Accepted: 6 February 2025

Published: 10 February 2025

Abstract: Perovskite solar cells (PSCs) are emerging as a promising technology for next-generation solar energy due to their high efficiency and cost-effectiveness. A critical step in the production of PSCs is the deposition of the perovskite absorber layer, the quality of which has a direct impact on the performance of device. Traditionally, quenching with an antisolvent is the main technique for the crystallization of such a perovskite film. However, gas quenching, an alternative approach in which pressurized gases (typically N_2) are used to supersaturate the perovskite precursor solution, has shown significant advantages. In contrast to quenching with antisolvents, gas quenching is more environmentally friendly, reduces chemical consumption, improves reproducibility, and offers better scalability for large-scale production. This review examines recent advances in gas quenching to produce high-quality perovskite films and compares the results with those achieved with antisolvent quenching. We highlight the performance benefits, environmental impact, and commercial scalability of gas quenching, and emphasize its potential to become the preferred method for industrial PSC production.

Keywords: perovskite solar cell; gas quenching; solvent annealing; large-area processing

1. Introduction

Perovskite solar cells (PSCs) have emerged as a revolutionary photovoltaic technology, marked by remarkable gains in power conversion efficiency (PCE), scalability, and economic feasibility. Over the past decade, lab-scale PSC efficiencies have surged from around 3.8% to over 26.7% [1] reaching levels that rival or even surpass those of conventional thin-film and silicon-based solar cells [2, 3]. In addition to single-junction cells, all-perovskite tandem devices have also garnered significant attention as the technology progresses [4]. This extraordinary advancement is due to the unique optoelectronic properties of perovskite materials, including high absorption coefficients, long carrier diffusion lengths, and tunable bandgaps, coupled with cost-effective fabrication methods [5–10]. However, achieving high efficiency and long-term stability in PSCs hinges on the production of high-quality perovskite films with precise control over crystallization and morphology. Challenges such as phase segregation and light sensitivity in perovskites remain key areas of concern [11]. Furthermore, the development of large-area fabrication processes is essential for the commercial viability of PSCs.

A key challenge in perovskite film fabrication is achieving precise control over the crystallization process during deposition. Most research on PSCs has relied on spin coating and antisolvent injection methods, commonly applied to traditional lead-based perovskites as well as lead-tin mixed and tin-based, lead-free compositions [12–20]. However, manual application of these methods introduces variability due to factors such as the deposition height, angle, and speed, which reduces reproducibility. Furthermore, scaling up these techniques for large-area, environmentally friendly production is challenging and often impractical [17, 19, 21, 22]. To overcome these limitations, researchers are increasingly exploring alternative strategies to improve control over perovskite film formation. Among these



methods, gas quenching has shown particular promise for optimizing perovskite crystallization and morphology, providing a more consistent and scalable approach to high-quality film fabrication.

Gas quenching, first employed during spin coating [23], utilizes an inert gas (such as nitrogen or argon) during the wet film deposition stage to rapidly remove residual solvents, thereby enabling controlled crystallization of the perovskite layer. This technique offers distinct advantages over antisolvent injection. By adjusting parameters such as gas flow rate, quenching duration, and substrate temperature, gas quenching provides precise control over nucleation and growth kinetics, resulting in smooth, pinhole-free films with large grain sizes and enhanced crystallinity—all with reduced solvent use. Additionally, gas quenching is compatible with scalable deposition techniques beyond spin coating, such as blade coating and slot-die coating, making it suitable for large-area applications [24–28].

Although very promising, the application of gas quenching in PSC research is still in its early stages, with many aspects of the technique yet to be fully explored. Key areas of ongoing investigation include optimizing quenching conditions, understanding the interplay between gas dynamics and film formation, and evaluating the effects of gas quenching on various perovskite compositions and device architectures. This review provides a comprehensive overview of the current state of gas quenching in PSC fabrication, discussing its fundamental principles, comparing it with other film formation techniques, and summarizing recent advancements. We also examine the impact of gas quenching on device performance, stability, and scalability, along with potential challenges and future directions for integrating this technique into large-scale, high-efficiency PSC production.

2. Nucleation and Growth

The nucleation and growth are decisive processes for film formation. Nucleation processes can be either homogeneous or heterogeneous. In the homogeneous nucleation, nuclei are formed without any preferred sites, whereas in heterogeneous nucleation, nuclei have preferred sites for formation. The homogeneity of the resulting film is directly linked with the size distribution of the nuclei. The formation of a smooth, pinhole-free perovskite film is essential for optimizing the performance of large-area PSCs. The LaMer model [29] highlights that the nucleation and crystal growth are more influential in determining film quality than the deposition process. As a result, the choice of quenching techniques, which drive the material into a supersaturated state, becomes pivotal in regulating nucleation and ensuring proper crystal development [30]. The rate and amount of nucleation are influenced by factors such as solution concentration, temperature, reaction time, and the degree of supersaturation, the latter being the key determinant. Following nucleation, these initial nuclei grow in the supersaturated solution, forming larger crystals. Achieving high nucleation rates before significant growth occurs is essential for producing perovskite films with high coverage and minimal number of defects. The ideal approach is to promote rapid nucleation while simultaneously suppressing growth, as this helps produce dense, defect-free films. Liu et al. modeled nucleation rates and demonstrated that supersaturation, temperature, and surface free energy are primary factors influencing nucleation, with the temperature affecting precursor volatilization and crystallization mainly driven by saturation levels [31]. Zhaojin et al. explained nucleation for using large area solar modules using slot die/blade coating [32]. They showed that high temperatures can reduce the nucleation energy barrier, increasing the nucleation rate and resulting in more crystal nuclei. Seulki et al. used hot air quenching during spinning and found out that hot quenching could give uniformly distributed nuclei [33]. However, controlling the temperature is vital, as excessive nucleation can lead to defects.

3. Developments in Antisolvent Methods

One effective strategy for controlling nucleation and growth is the antisolvent engineering. The role of an antisolvent is to be miscible with the solvent but with the desired final material being insoluble in it, causing a rapid transition from an unsaturated to a supersaturated state, thereby inducing crystallization. Selecting the right antisolvent depends on parameters such as polarity and boiling point. Ideally, an antisolvent should have a polarity between 2.0 and 4.5. Higher polarity increases perovskite solubility, resulting in lower precipitation and poorer film coverage. However, low-polarity antisolvents can cause unstable precursor solutions, slower diffusion rates and issues with grain formation, leading to impurities and defects that degrade film quality and device efficiency. The boiling point is another important factor: low boiling points lead to rapid evaporation, potentially resulting in fast film formation with small crystals, while high boiling points can prolong solvent presence, causing incomplete crystallization. Selecting an antisolvent with balanced polarity and boiling point is key to achieving uniform, high-quality films [34].

Antisolvent engineering primarily focuses on two-dimensional film crystallization, but three-dimensional growth behavior is also critical. Zheng et al. explored the crystallization dynamics in various perovskite films

using glow discharge optical emission spectroscopy (GD-OES), X-ray diffraction (XRD), and scanning electron microscopy (SEM), identifying three distinct growth trends upward, downward, and lateral after annealing, with lateral growth being the fastest [35]. In another study, Chen et al. observed top-down growth in methylammonium lead iodide (MAPbI₃) films when treated with a mixture of dimethylformamide (DMF) and dimethyl sulfoxide (DMSO) using chlorobenzene (CB) as an antisolvent. The intermediate phase transitioned from the top layer downward, driven by DMSO evaporation, completing crystallization within 10 min, independent of perovskite composition [36].

The antisolvent dripping technique involves the gradual addition of a defined volume of antisolvent onto the developing perovskite layer during the spin coating process. In a landmark study from 2014, Xiao et al. introduced a fast deposition-crystallization (FDC) method that utilized various solvents—such as CB, toluene, benzene, xylene, methanol, ethanol, 2-propanol, ethylene glycol, tetrahydrofuran (THF), chloroform, benzonitrile, and acetonitrile (ACN) as antisolvents for perovskite layers. During this FDC process, the antisolvent was applied to the spinning perovskite substrate just seconds after the initiation of spin coating [37]. This approach resulted in an immediate darkening of the film, indicating a rapid crystallization process, whereas conventional spin coating typically required thermal treatment at approximately 100 °C for crystallization to occur. Among the solvents tested, CB, benzene, xylene, and toluene were particularly effective, yielding uniform films and complete surface coverage. Notably, MAI, PbI₂, and MAPbI₃ demonstrate low solubility in these solvents. The use of antisolvents caused immediate supersaturation, reducing the solubility of perovskite precursors, which in turn facilitated rapid crystallization and film formation during spin coating. Conversely, solvents that dissolve the perovskite precursors to a high or moderate degree—such as methanol, ethanol, ethylene glycol, ACN, THF, and benzonitrile—produced undesirable results, including large PbI₂ crystals or transparent films. The SEM images of the perovskite films fabricated via antisolvent injection and conventional spin coating are given in Figure 1c. The images demonstrate improved coverage and uniformity of the perovskite film after antisolvent injection whereas the lack of it leads to non-uniform crystallization. The optimized devices, with a perovskite layer thickness of 350 nm, that were fabricated using CB as an antisolvent achieved an impressive average PCE of $13.9 \pm 0.7\%$, surpassing the efficiencies of other contemporary fabrication methods. This enhancement in PCE is attributed to the uniform film coverage and the absence of pinholes in the perovskite absorber layer. This improved film quality led to better light absorption and fewer defects, contributing to enhancements in short-circuit current density (J_{SC}) and V_{OC} .

Meanwhile, Jeon et al. investigated the use of toluene as an antisolvent for perovskite film formation, particularly when mixed with other solvents such as DMF, DMSO, and γ -butyrolactone (GBL) [38]. They deposited MAPb(I_{1-x}Br_x)₃ perovskite precursors, which were dissolved in a GBL-DMSO mixed solvent, onto a bilayer TiO₂ substrate using spin-coating, followed by toluene dripping and a 10-minute annealing at 100 °C to form the perovskite film. The resulting toluene-dripped perovskite film exhibited uniformity and reduced roughness, achieving full surface coverage. In contrast, films without toluene dripping displayed non-uniformity and insufficient coverage. XRD analysis indicated no significant differences in crystallinity between the two types of perovskite films. The PSCs created using bilayer TiO₂, GBL-DMSO solvent, and toluene dripping reached an average PCE of 16.5%.

Notably, the perovskite film formed through an intermediate phase (MAI-PbI₂-DMSO) upon the addition of toluene during spin coating required additional thermal treatment at elevated temperatures to eliminate DMSO molecules from the intermediate phase and obtain a pure perovskite film [38, 39]. Consequently, toluene dripping facilitated slower crystallization, resulting in larger (yet adequately dense) grains of perovskite compared to those produced via direct crystallization with other antisolvents (like CB). Toluene treatment also encouraged the formation of smoother MAPbI₃ films with better surface coverage on noncrystalline substrates made from poly(3,4-ethylenedioxythiophene) polystyrene sulfonate (PEDOT:PSS) [40]. As a result, these films exhibited significantly increased absorption; however, exciton dissociation efficiency slightly decreased due to smaller grain sizes compared to non-treated films.

Ahn et al. showed the effect of Lewis base adduct of lead iodide, namely PbI₂.DMSO together with DEE injection on the performance of perovskite films and PSCs [41]. By this strategy they increased PCE of their devices to an average of $\sim 19.7\%$ from an average of $\sim 18.3\%$. Figure 1a shows the illustration of their perovskite fabrication routes and the corresponding SEM images to show the improved film quality due to DMSO addition to the perovskite solution and DEE injection during spin coating. By using a similar Lewis base adduct strategy, Lee et al. paired Lewis base DMSO with NMP to form a stable intermediate adduct phase, which later transforms into a uniform and pinhole-free FAPI film [42]. For FAPI, NMP adduct is found to be more effective than a DMSO based adduct due to stronger interaction of formamidinium (FA) cation with NMP compared to DMSO. This improved film quality leads to a PCE of over 20% and an average PCE of $18.83 \pm 0.73\%$. Figure 1b shows the illustration of

perovskite film formation via Lewis base X which can be DMSO or NMP, and the photographs and SEM images of the resulting perovskite films.

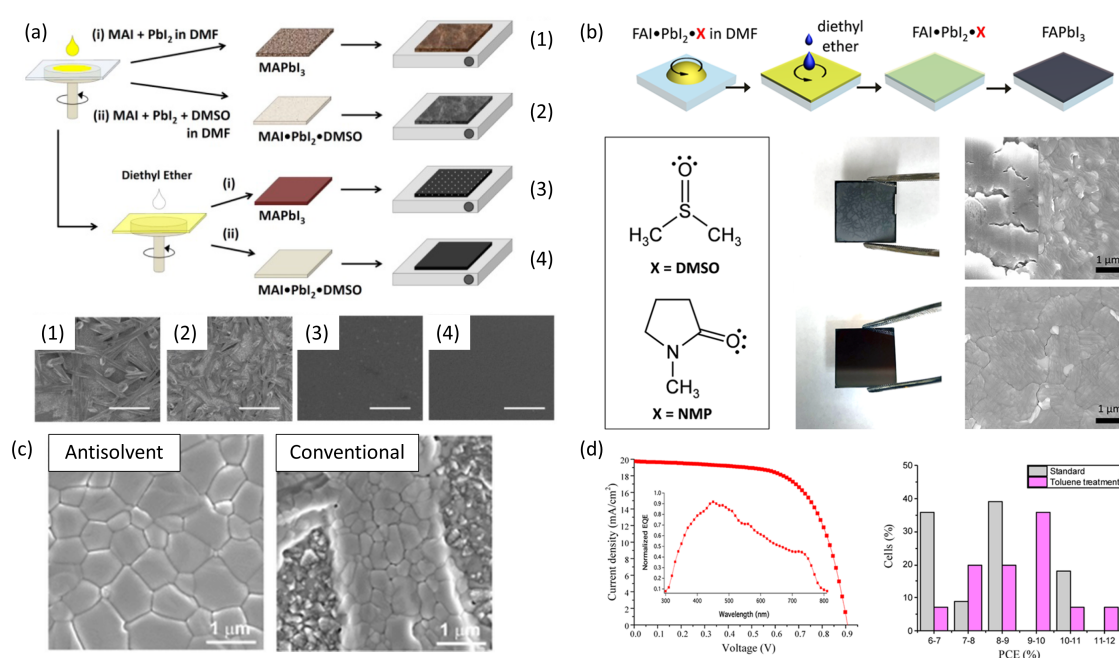


Figure 1. (a) Illustration of the fabrication procedure and the resulting SEM images for MAPbI₃ films obtained via spin coating from DMF-based perovskite precursor solution with (1) methylammonium iodide (MAI) and PbI₂, (2) MAI, PbI₂, and DMSO (3) 1st solution (with MAI and PbI₂) with Diethyl ether (DEE) injection, and (4) 2nd solution (with MAI, PbI₂, and DMSO) with DEE injection. Reprinted with permission from [41]. Copyright 2015 American Chemical Society. (b) Illustration of formamidinium lead iodide (FAPbI₃) film fabrication with Lewis bases and effects of DMSO and N-Methyl-2-pyrrolidone (NMP) as Lewis bases on FAPbI₃ films shown by photographs and SEM images. Reprinted with permission from [42]. Copyright 2018 American Chemical Society. (c) SEM images of MAPbI₃ films prepared via FDC method with CB as antisolvent and with no antisolvent injection. Reprinted with permission from [37]. (d) I-V curve obtained from HTM-free PSC that was fabricated via toluene antisolvent injection and the statistical comparison of PCE of PSCs with toluene injection and no antisolvent. The statistical analysis include results from 84 cells. Reprinted with permission from [43]. Copyright 2016 American Chemical Society.

Interestingly, perovskite materials can function both as photon absorbers and hole transporters, leading to simpler device architectures that do not require hole conductors, making them efficient and cost-effective [44, 45]. The quality of the contact between perovskite and metal is crucial for effective charge collection and transport. The use of toluene as an antisolvent resulted in fewer pinholes and a smoother surface on the perovskite film, which enhanced the optoelectronic properties and improved the perovskite-metal interface, thus enhancing device performance and minimizing hysteresis [43] Figure 1d. It was hypothesized that the surface ions (halide and methylammonium) formed a complex with the solvent, which was removed during toluene dripping, resulting in a net positive charge on the Pb atoms and promoting the formation of high-quality perovskite films [43].

As demonstrated with these examples, it turns out that the film crystallization strongly depends on the used solvent/antisolvent and has to be optimized for every perovskite composition. Also, parameters, such as amount of solvent, timing of exposure to the solvent and length of exposure time all play an important role for the final film quality. It is therefore not only time consuming to find the ideal parameter space for the film preparation, but also faces often some reproducibility issues, as for example small changes in environmental conditions (e.g., different conditions in glovebox due to evaporated solvents) and timing can have significant influence on the final perovskite film quality.

4. Mechanism of Perovskite Film Fabrication via Gas Quenching

The mechanism of both quenching methods i.e antisolvent quenching and di gas quenching is quite different. In gas quenching no extra solvent is added to dry the precursor solvent. Instead it is dried with an air knife/gas nozzle (compressed air, inert gas) to initiate the crystallization. The focus during quenching is on sweeping the solvent vapors away to accelerate the evaporation rate [30].

The perovskite solution on the substrate is rapidly dried by forcing a gas, such as nitrogen or argon gas, over the substrate. The efficiency of this process is primarily determined by the airflow geometry, while the specific gas used for drying plays a minimal role. This is because different gases behave similarly as ideal gases in this context. To identify the key parameters for gas quenching, consider the setup illustrated in Figure 2. The gas is ejected with a velocity u_0 , from a nozzle with a width D , positioned at a height H and angled at θ over the substrate. The nozzle can be either a round or slot type. These experimental parameters enable the use of established correlations to predict the local mass transfer coefficient of the solvent into the gas phase. With these parameters, setups can be directly compared [46]. Other factors such as gas pressure, are unnecessary because they depend on the specified parameters in a complex way. The solvent is then present in the gas phase with a certain concentration of gaseous solvent. The concentration jump at the phase boundary can be described by Raoult's law. It describes that the partial pressure of each component of an ideal mixture of liquids is equal to the vapor pressure of the pure component (liquid or solid) multiplied by its mole fraction in the mixture.

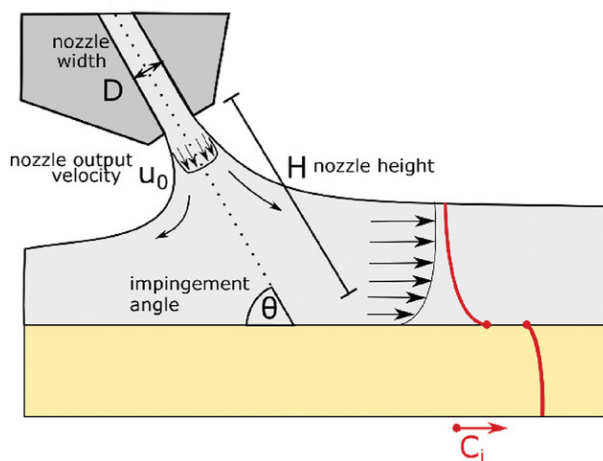


Figure 2. Gas quench mechanism. Reprinted with permission from [46].

Moreover, the integration of computational techniques, such as computational fluid dynamics (CFD), can help to improve the design and optimization of quenching processes as demonstrated for many industrial processes. These advancements allow for precise control over cooling rates and patterns, minimizing distortions and improving material properties. CFD has proven to be a valuable tool to optimize the parameters for practical applications, driving significant enhancements in quenching performance and outcomes [47]. Unlike the antisolvent method, supersaturation in the gas quenching process is induced solely by rapid solvent evaporation, which increases solute concentration without concurrently reducing solubility as in the antisolvent technique. This results in a milder supersaturation during gas quenching, providing an extended processing window for precise control over the intermediate film. Such conditions promote uniform nucleation, ensuring the formation of a highly homogeneous perovskite film [21, 48, 49].

Optimized pressure during gas quenching is one important aspect for upscalability. Very high pressure could cause cracks and very low pressure could cause non-uniform films. Therefore desired range for pressure for gas quenching should be considered. Achieving high-quality Formamidinium-Cesium-based perovskite films often requires MA-containing additives, which can compromise long-term stability. Additionally, the gas-quenching process for FA-based perovskites demands high pressure, limiting its practicality, especially for MA-free materials. Reducing this pressure requirement remains a key challenge. The optimized gas pressure for FA based perovskites is significantly higher than that of MA based perovskites [50]. Reducing gas pressure yet getting the uniform films could be a limitation to this process. Tian et al. used tetramethylene sulfoxide (TMSO) as a ligand instead of MA based cations to get the low pressure yet uniform films [51].

5. Gas Quenching for Spin Coating

Gas quenching was first introduced by Huang et al. for MAPbI₃ thin films, achieving a PCE of 17.0% and establishing the technique as a valuable method for perovskite film formation [23]. This method has since then widely been studied and applied to various perovskite compositions and fabrication processes. Conings et al. demonstrated its use with DMSO-based solutions, leading to the formation of pinhole-free perovskite layers [52]. The versatility of gas quenching is further evidenced by its successful implementation for diverse perovskite compositions with different bandgaps, showcasing its adaptability for different material systems relevant to high-efficiency solar cells.

Several groups have explored advanced additive and solvent engineering strategies using gas quenching to further optimize perovskite films and solar cell performance. For instance, Babayigit et al. achieved an average PCE of 19.7% in RbCsFAMA-based quadruple-cation PSCs using gas quenching [53], while Tang et al. used n-hexylammonium bromide for surface passivation, resulting in a remarkable PCE of 23.6% with KI-incorporated films [54]. In a related study, Zhang et al. employed bithiophene propylammonium iodide (bi-TPAI) to enhance the surface properties of gas-quenched perovskite films, boosting the PCE from 20.0% to 22.0% [55]. Wu et al. also reported the effective use of gas quenching in Sn-containing perovskite films for TSCs, achieving a PCE of 25.23% by combining narrow and wide bandgap perovskites [56]. Meanwhile, Heydarian et al. demonstrated the potential of gas quenching in triple-junction TSCs, fabricating a top perovskite layer with a record open-circuit voltage (V_{OC}) of over 2.8 V [57].

Gas quenching has proven to be effective across a variety of solvent systems and perovskite compositions. Brinkmann et al. applied it to an NMP/DMF solvent system, achieving uniform, well-crystallized MAPbI₃ and CsFA double-cation perovskite films with PCEs of up to 18.5% [58]. They claimed that DMSO results in dewetting of the perovskite precursor solution on hydrophobic hole transport layers (HTLs) during gas quenching process Figure 3b. On the other hand, using NMP instead of DMSO as co-solvent alongside DMF fixes this issue due to its lower hydrophilic-lipophilic balance. Szostak et al. compared the effects of NMP and DMSO solvents on perovskite crystallization, showing that NMP-based films achieved superior morphology and PCEs compared to their DMSO counterparts [59]. They used in-situ grazing incidence wide angle X-ray scattering during gas quenching while spin coating. This way, they were able to track the formations of the intermediates and the perovskites. Their measurements during spin coating is given in Figure 3c. Similarly, Sun et al. used pyrrolidone-based ligands with gas quenching to fabricate CsFAPbI₃ films, optimizing the buried interfaces and achieving a PCE of 21.6% [60]. This demonstrates that gas quenching is compatible with a wide range of solvents and compositions, making it highly versatile for various perovskite formulations.

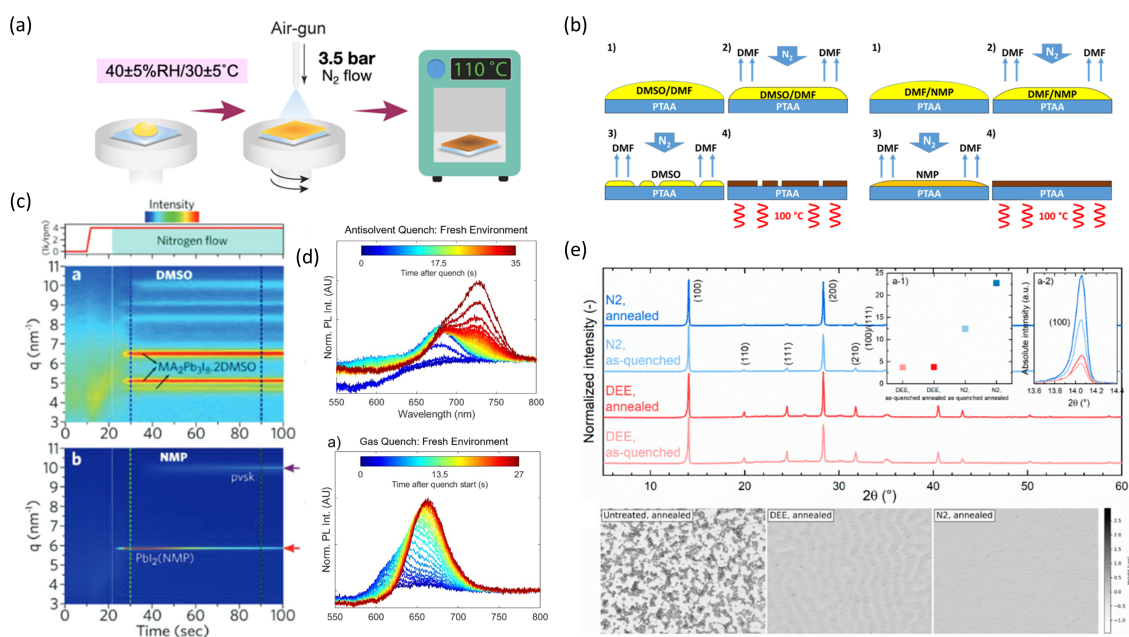


Figure 3. (a) Illustration of perovskite film fabrication via gas quenching under $40 \pm 5\%$ RH/ $30 \pm 5^\circ\text{C}$. Reprinted with permission from [61]. Copyright 2023 American Chemical Society. (b) Illustration of the proposed schematics demonstrating the drying and dewetting for DMSO and NMP co-solvents. Reprinted with permission from [58]. Copyright 2019 American Chemical Society. (c) In-situ time-resolved X-ray scattering intensity maps for MAPbI₃ films showing the effect of having DMSO and NMP in perovskite precursor solution on film formation [59]. (d) In-situ PL measurement results showing the perovskite evolution in fresh environment for antisolvent quenched and gas-quenched films. Reprinted from [21]. (e) XRD patterns and optical profilometry images of perovskite films fabricated via N₂ quenching (blue on XRD pattern) and DEE quenching (red on XRD pattern). The left inset shows the (100)/(111) peak intensity ratios from each sample while right inset shows the comparison of (100) peak intensities from each sample. Reprinted with permission from [62]. Copyright 2020 American Chemical Society.

There are also examples of gas quenching being applied to different device architectures and applications. For instance, Zhang et al. achieved PCEs of 24.3% and 22.6% in inverted PSC using 2-thiophene-ethylammonium chlo-

ride (TEACI) for interfacial modification [63]. Song et al. investigated the impact of formamidinium chloride (FACI) and methylammonium chloride (MACI) on perovskite film properties, highlighting the role of A-cation halides in regulating film stability [64]. Other studies, such as those by Ocebe et al., applied gas quenching to fabricate double perovskite films like $\text{Cs}_2\text{AgBiBr}_6$, exploring its effect on film morphology and device performance [65, 66]. In addition, Werner et al. focused on MA-free Sn-Pb perovskite films, finding that gas quenching enhanced film quality and eliminated defects like wrinkling [62]. Figure 3e shows the comparison between XRD patterns and morphology of Sn-Pb perovskite films fabricated by DEE quenching and N_2 quenching. The XRD pattern comparison shows that N_2 quenching improves the crystal orientation of Sn-Pb perovskite films while reducing the wrinkles on the final film surface.

The timing of flow of nitrogen seems to be less critical in comparison to anti-solvent quench [58, 62, 67] which could be one reason for its known better repeatable results [51]. Recent advancements include the development of automated and environment-controlled gas quenching systems. Kaczaral et al. implemented an automated gas quenching system with in-situ photoluminescence (PL) monitoring, ensuring consistent film quality and minimizing human error [21]. They compared the PL evolution during or after antisolvent injection and gas quenching while spin coating. Figure 3d shows the PL evolution of antisolvent injected and gas-quenched perovskite films in fresh environments as a function of time. They showed that gas quenching always gives the same type of perovskite film formation regardless of the atmosphere whereas antisolvent quenching may result in different perovskite film formation depending on the atmosphere or over time. Their study shows that gas quenching gives more repeatable results as compared to anti-solvent quench as shown in Figure 4. Harnmanasvate et al. explored gas quenching under high-humidity conditions, using urea as an additive to form stable, high-quality CsFA perovskite films with larger grain sizes and enhanced stability [61] Figure 3a. Cassella et al. used a high-vapor pressure solvent mixture and room-temperature gas quenching to fabricate MAPbI₃ films without the need for an annealing step, achieving a PCE of up to 18.0% compared to the device with annealed perovskite with 18.4% [68].

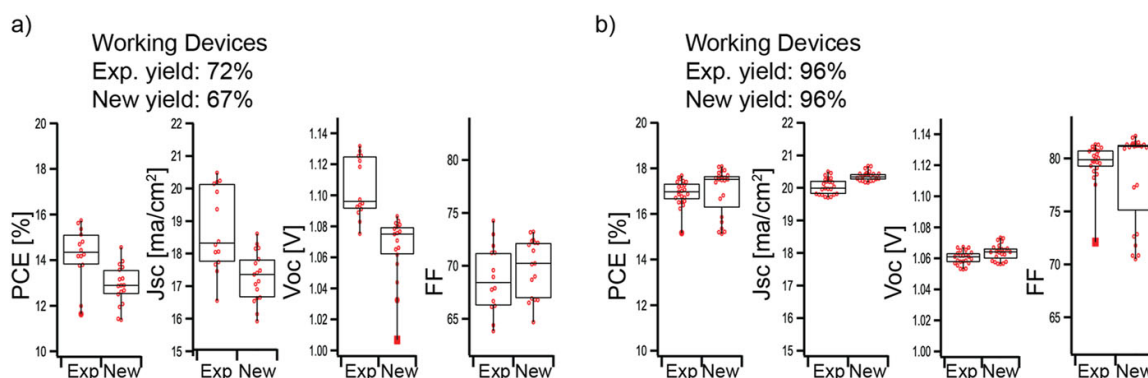


Figure 4. Device metrics between an expert (Exp) and a novice (New) device maker for p-i-n devices made by the (a) antisolvent method and (b) automated gas quenching method. Reprinted with permission from [21]. Copyright 2023 APL Energy.

Overall, gas quenching has established itself as a robust technique for the fabrication of high-quality perovskite films fabricated via spin coating, enabling diverse applications and consistent performance enhancements across multiple perovskite compositions, solvent systems, and device architectures. However, spin coating is not a viable method for large area solar cells. Nonetheless, gas quenching can be adapted to large area deposition methods, which we will be discussed in the following sections.

6. Gas Quenching for Large Area Fabrication Methods

6.1. Blade Coating

Blade-coating is a widely utilized method for fabricating large-area PSCs. The continuous film-forming process relies on the movement of the blade across the solution to facilitate the formation of large grains. However, due to the flow and diffusion of the solution during the blading process, non-uniform films are prone to form. To address these issues, gas quenching-assisted blade coating can be employed to obtain a more uniform film. Basically there is a blade coater followed by rolling nitrogen knife as shown in Figure 5a. After the solution is applied to the substrate, the gas blade spreads the solution, accelerates solvent evaporation and induces nucleation in the wet film. This approach has shown to significantly improve the performance of large-area devices by optimizing processing parameters, such as air velocity, air temperature, and substrate temperature.

The potential of gas quenching for large-area module fabrication was highlighted by Razza et al. They prepared lead iodide (PbI_2) films using air-assisted blade coating, achieving 10.1 cm^2 modules with a remarkable PCE of 10.4% [69].

Invention of air assisted blade die coating or shortly referred here as air-blade method comes with a lot of challenges and issues that gained attention of researchers and are solved one by one by various interesting approaches. Here we stated a few of them.

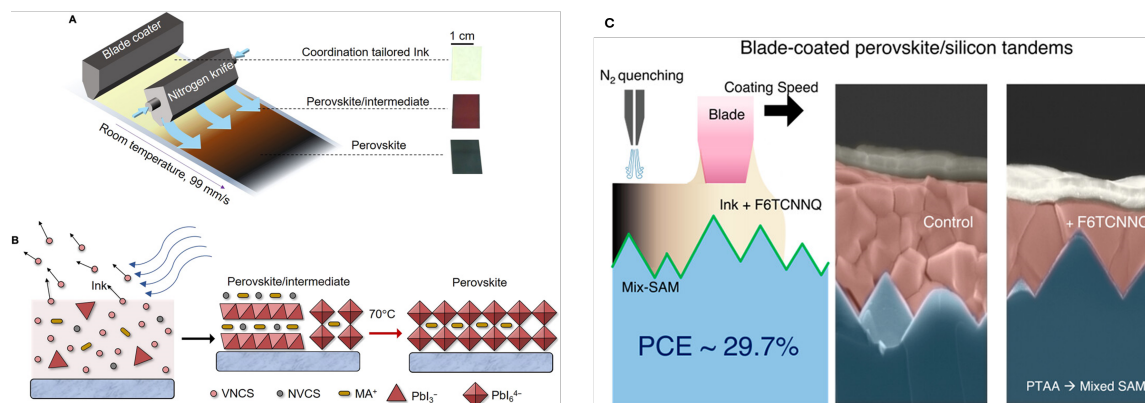


Figure 5. (a) Schematic illustration for N_2 -knife–assisted blade coating of perovskite films at 99 mm/s at room temperature using coordination tailored ink. Copyright 2019 American Association for the Advancement of Science [24], (b) Schematic illustration showing the drying of ink into a perovskite/intermediate film and full crystallization of a perovskite film where VNCS is volatile non-coordinating solvent and NVCS is non-volatile non-coordinating solvent. Copyright 2019 American Association for the Advancement of Science [24], (c) Diagrammatic representation of blade coating with effect of dopant molecule. Reprinted with permission from [25]. Copyright 2024 American Chemical Society.

Blade coated films face the challenge of fast deposition and low crystallinity. Crystallization of perovskite is also linked with the coordinating solvent. When perovskite solution ink reaches the surface of substrate, it forms an intermediate of perovskite with solvent as shown in Figure 5b. Yehao et al. demonstrated that while common solvents like DMSO and DMF hinder fast, smooth perovskite film deposition at room temperature, highly volatile solvents such as 2-Methoxyethanol (2-ME) and ACN lead to films with low crystallinity and poor substrate contact but film deposition is fast. By combining these solvents in a specific ratio, they managed to overcome these limitations and addressed the issue of achieving uniform perovskite films at a high deposition speed of 99 mm/s, producing modules with efficiencies above 16% on areas over 60 cm^2 [24]. The airflow temperature also plays a vital role in uniform film formation and film quality. Various airflow temperatures such as 50, 100, and 150 °C were analyzed. At an airflow temperature of 100 °C, the film displayed a more homogeneous surface with large grains and low roughness, yielding a PCE of 14.8% for a 0.71 cm^2 device [33].

Another challenge for this technique are film thickness variations due to short-distance airflow blowing. To mitigate these problems, Gao et al. proposed a multiflow air knife (MAK) method [70]. The wet film is dried using MAK and heated for 10 min, producing a dense, compact film with a surface roughness of 4.9 nm over a $10 \times 10 \mu\text{m}^2$ scan area. Such uniform films result from optimizing airflow and air knife-to-liquid distance, achieving a PCE of 17.71% for a 0.1 cm^2 device. They further investigated the effects of airflow rate and temperature on boundary layer thickness, finding that high air velocity and low temperature accelerated solvent evaporation, improving film quality [71].

Moreover, the drying time of perovskite ink also needed attention. Because, given the fast blading speeds and low deposition temperatures, perovskite ink does not dry immediately. Solvent properties, including viscosity, volatility, and vapor pressure also influence film formation. Deng et al. explored the use of volatile-non-coordinating solvents (VNCS), nonvolatile-coordinating solvents (NVCS) and their combinations for room-temperature N_2 -assisted blade coating [24]. They found that a 98% volume mixture of VNCS with DMSO achieved rapid drying and large perovskite grains. This setup yielded a small-area device PCE of 21.3% and a module PCE of 16.4% for a 63.7 cm^2 aperture area.

Other developments includes additive engineering which is a well-established method for modulating film morphology, suppressing non-radiative recombination, and passivating defects, thereby improving device performance. Precursor engineering is also essential for producing high-quality perovskite films using gas quenching-assisted blade coating. A mixed MAI/MACl precursor was used to delay crystallization, resulting in smooth films with

enhanced crystallinity, fewer vertical grain boundaries and lower trap-state densities [72]. The resulting device achieved a PCE of over 19.0%. Gao et al. introduced lead acetate ($\text{Pb}(\text{Ac})_2$) and guanidinium (GA) cation into the precursor, controlling crystallization through the byproduct methylammonium acetate (MAAc), which increased the crystallization rate. The resulting $4.8 \times 9.6 \text{ cm}^2$ device based on $\text{GA}_{0.12}\text{MA}_{0.88}\text{PbI}_3$ exhibited a PCE of 19.44%, and a semi-module with a 16 cm^2 active area showed a PCE of 13.85% [73]. Adding 5% lead thiocyanate ($\text{Pb}(\text{SCN})_2$) to the precursor improved grain size, carrier lifetime, and crystallinity, yielding a PCE of 20.08% for a 0.09 cm^2 device. Dai et al. added NH_4Cl to delay nucleation, producing high-quality films and achieving a PCE of 15.86% on a flexible substrate [74]. Jaehoon et al. continued with idea of precursor engineering and used a solution composed of 2-ME and 1,3-dimethyl-imidazolidinone (DMI), which exhibits enhanced intermediate phase stability and facilitates the scalable production of efficient perovskite solar modules. Using this precursor solution, uniform, pinhole-free perovskite films were successfully deposited over areas exceeding 100 cm^2 , yielding higher-efficiency PSCs and modules. The optimal unit cell and module configurations, utilizing an n-i-p structure, achieved power conversion efficiencies of 23.4% and 20.1% respectively. A variety of non-destructive metrology techniques, including spectroscopic ellipsometry, hyperspectral PL, electroluminescence, and laser beam-induced current mapping, were employed to assess and refine the development of blade-coated perovskite modules. These results underscore the potential of rationally engineered precursor inks for blade coating in the scalable production of efficient perovskite solar modules [75]. Anand et al. introduced a molecular dopant 2,2'-(perfluoronaphthalene-2,6-diylidene)dimalononitrile (F6-TCNNQ) in the precursor ink, facilitating the formation of micrometer-thick perovskite films compatible with textured silicon bottom cells. By also reducing the energy mismatch between the hole-selective contact and the perovskite, they achieved a record tandem efficiency of 29.7% shown in Figure 5c. Other than precursor engineering, additives in solvent could also be helpful for high quality films. Ethanol cosolvent strategy was performed by incorporating ethanol into perovskite ink for high-performance, room-temperature blade-coated PSCs and modules. Real-time crystallization studies reveal detailed structural evolutions and phase-transition pathways in the perovskite. Time-resolved XRD and density functional theory (DFT) calculations show that ethanol in the mixed-solvent system promotes the formation of a FA-based precursor solvate ($\text{FA}_2\text{PbBr}_4 \cdot \text{DMSO}$), which finely tunes the nucleation-crystal growth balance to yield high-quality perovskite films. This method effectively suppresses non-radiative recombination, achieving efficiencies of 23.19% for a 1.54 eV perovskite system and 22.51% for a 1.60 eV system, representing some of the highest efficiencies for blade-coated PSCs in both small-area devices and mini-modules. The device exhibits an exceptionally low V_{OC} deficit of 335 mV and a non-radiative recombination loss of just 77 mV. Additionally, this strategy significantly enhances device stability, making it a promising approach for high-efficiency, stable PSCs [76].

For fabricating intrinsic transparent formamidinium lead bromide (FAPbBr_3) perovskite films, Wang et al. present an intermediate-phase-transition-assisted one-step blade coating method. The intermediate complex enhances crystal growth, yielding homogeneous, large-area absorber films. The champion device achieves a PCE of 10.86% with a V_{OC} of 1.57 V, utilizing a glass/FTO/ SnO_2 / FAPbBr_3 /carbon architecture. Unencapsulated devices retain 90% of their initial efficiency after 1000 h at $75 \text{ }^\circ\text{C}$ in ambient air and 96% after 500 h of maximum power point tracking. Printed semi-transparent PSCs exhibit efficiencies of 8.6% for small devices and 5.55% for $10 \times 10 \text{ cm}^2$ modules, with over 45% average visible light transmittance. The customizable color, transparency, and thermal insulation properties of FAPbBr_3 PSCs highlight their potential as multi-functional BIPVs [77].

A very eco friendly strategy was opted by Farshad et al. by not using any toxic solvents and they presented sustainable flexible perovskite solar modules (flex-PSMs) fabricated entirely via blade coating in ambient air. A double-cation $\text{Cs}_{0.15}\text{FA}_{0.85}\text{PbI}_{3-x}\text{Br}_x$ perovskite is blade coated in two steps, with optimized drying conditions in the first step critical for obtaining high-quality films with the desired perovskite phase. Through additive engineering, they improved the morphology and reduced voids, achieving an efficiency of 14%. Furthermore, 94 cm^2 modules demonstrate the scalability of the fabrication process [78].

$\text{FA}_{0.6}\text{MA}_{0.4}\text{Pb}_{0.4}\text{Sn}_{0.6}\text{I}_3$ PSCs, yielding an efficiency of 18.3% and a V_{OC} of 0.845 V [79]. 2ME-based $\text{Cs}_{0.05}\text{FA}_{0.95}\text{PbI}_3$ ink using pre-synthesized single crystals was formulated for fabricating intrinsic transparent FAPbBr_3 perovskite films, which eliminates colloidal particles and suppresses colloid-induced heterogeneous nucleation, promoting larger grain growth and improved film crystallinity. The precursor-engineered ink is employed in vacuum-free, fully printed solar cells with carbon electrodes, yielding a PCE of 19.3% and a T_{80} (80% of initial PCE) of 1000 h in the ISOS-L-2I ($85 \text{ }^\circ\text{C}/1 \text{ Sun}$) aging test. This methodology also enables the production of carbon-electrode mini solar modules with a stabilized PCE of 16.2% (average 15.6%), achieving a record for fully printed devices and advancing scalable photovoltaic technology [80]. Tian et al. introduced a low-temperature processable ink for FAPbI_3 perovskite, free of MA- and Cs-containing additives, suitable for producing large-area perovskite films via blade-coating under ambient conditions [81]. Despite of all those advancements blade-coated

PSCs compared to spin-coated devices, often exhibits lower PCE due to sensitivity to morphology and crystallization kinetics. To overcome this problem, an air-knife-assisted ambient fabrication of PSCs at a relative humidity of $55 \pm 5\%$ using a DMF-DMSO solution was used. Time-resolved UV–vis spectrometry analyzes solvent removal and crystallization rates, crucial for optimizing morphology. The antisolvent-free PSCs achieve PCEs of 21.1% for 0.06 cm^2 devices and 18.0% for 1 cm^2 devices, with stability comparable to those made in glovebox conditions. These findings demonstrate the potential of high-humidity ambient coatings for scalable PSC production [30].

Precursor solution dewetting and complex quenching issues were resolved by Johannes et al. They presented a one-step blade coating method for inverted (p-i-n) double-cation PSCs using DMSO at low temperatures. A blade-coated wetting agent of silicon oxide nanoparticles is applied to the hydrophobic HTL to prevent dewetting and gas stream-assisted drying is used for effective quenching. The DMSO-coated PSCs achieve PCEs of 16.7% on a 0.24 cm^2 active area, comparable to 16.9% from a DMF mixture, demonstrating that DMF is unnecessary. This advancement brings PSCs processed with environmentally friendly solvents closer to industrial implementation [82].

In situ optical spectroscopies were integrated into a doctor-blading setup to monitor film formation in real-time during gas quenching. Results show that gas quenching is vital for producing smooth and compact perovskite films by controlling the nucleation rate. Phase-field simulations further reveal that excess MAI increases grain size by accelerating crystal growth rates. Ultimately, optimized crystal growth control leads to fully printed solar cells with a champion PCE of 19.50% and mini solar modules with 15.28% efficiency [83].

Automation is one big step towards upscaleability and commercialization of solar cells. Semi-automated, scalable blade-coating method was investigated for gas-quenched blade die coating. Luigi et al. fabricated perovskite solar modules in ambient conditions, using a triple-cation cesium methylammonium formamidinium perovskite. The two-step deposition process, assisted by air and green antisolvent quenching, enables the production of small-area cells with over 17% efficiency and highly reproducible modules (less than 2% variability) with a 90% geometrical fill factor and efficiency greater than 16%. The modules show high stability, with a T80 lifetime of 750 h under light-soaking conditions at maximum power point and room temperature after encapsulation. Characterization techniques, including SEM, profilometry, UV-vis and PL spectroscopy, and electroluminescence imaging, confirm improved film quality with fewer defects in ambient air-fabricated devices compared to nitrogen-based spin-coated devices, supporting the potential of this process for scalable PSC production [84].

After the semi automated, scalable blade coating model by Luigi et al. in 2021, they came up with perovskite sub-modules of (320 cm^2 total area, 201 cm^2 aperture area, 93% geometrical fill factor) fabricated in ambient air using a hybrid meniscus coating technique combined with air and green antisolvent quenching. To reduce non-radiative recombination, enhance carrier extraction and control perovskite growth over large areas, phenethylammonium iodide (PEAI) passivation and solvent-addition strategies were employed. The resulting sub-modules achieved 16.13% efficiency, with just 7% efficiency loss compared to small-area cells and no loss relative to mini-modules, along with stability exceeding 3000 h based on ISOS-D-1 standards for dark storage/shelf life in ambient conditions. A life cycle assessment demonstrated the sustainability of the materials and methods, showing that scaling up operations mitigates environmental impacts and enhances resource efficiency. Furthermore, economic analysis indicates a significant cost reduction of about 40% when scaling from mini- to sub-modules [85].

After all those advancements in air blade method, it can be considered as one competitive method. It can be used to deposit electron transport layers (ETLs) and HTLs, simplifying the process and enhancing performance [86].

Generally, blade coating technique is considered to be an upscalable deposition technique but with antisolvent this upscalability is questionable. Gas quenching seems to be a competitive option as an alternate to anti-solvent for blade coating. Non-uniformity of films due to solution flowing issues is one limitation of blade coating which could be improved using gas quenching. If the gun distance to the substrate is too small, it might cause some strain in films leading to pin-holes and cracks in the films. A better fine tuning of the fabrication parameter to get uniform films with air blade method is still required.

6.2. Slot-Die Coating

The slot-die coating process was developed by Beguin at Eastman Kodak Company to address the limitations of conventional coating techniques, such as ink waste and slow coating speeds in the production of films or photographic paper [87].

Solution-coating processes offer a cost-effective approach for producing active layers in the industrial development of perovskite solar devices. Among these methods, scalable techniques stand out for their ability to deliver uniform coatings with minimal defects across large areas at high speeds. Slot-die coating is a key example, involving the controlled deposition of liquids or solutions onto either a stationary or moving substrate through a meniscus coating process.

In a typical slot-die coating method, perovskite ink flows onto a moving substrate through a narrow opening in the slot-die head. When the ink contacts the substrate, it forms two menisci, one upstream and one downstream of the coating bead. The wet film then gradually extends along the coating path, guided by the downstream meniscus. Slot die coating could be effectively paired with gas quenching by optimizing the parameters such as quenching position, distance and velocity such as shown in Figure 6a. These parameters have a dominating effect on film morphology. Slot-die coating, when combined with gas quenching, can produce high-quality films and efficient PSCs. Cotella et al. optimized substrate temperatures and air knife application to reduce film roughness, achieving a PCE of 9.2% [88].

Like blade coating, slot die coating also sometimes faces the challenge of non-uniform films. Over the period of time various approaches have been reported to improve this issue. Here we state some of these efforts.

In 2018 Jueng et al. incorporated a blowing step into the slot-die coating method, significantly enhancing the coverage of the resulting perovskite films. Devices produced using the slot-die coating with the blowing technique achieved at that time a moderate PCE of 8.8%. Additionally, optimizing the deposition temperature further improved the morphology of the slot-die-coated perovskite films. The integration of both blowing and heating during the slot-die coating process, along with the implementation of a printing-friendly HTL, resulted in devices fabricated in ambient conditions achieving a PCE of 12.7% [89]. Lee et al. employed mixed lead precursors, specifically PbAc_2 and PbCl_2 , to fabricate perovskite films with good crystallization and uniformity using nitrogen-assisted slot-die coating. This method effectively mitigates the challenges of morphology control typically associated with single lead sources. A module with a total area of 10 cm^2 successfully achieved a PCE of 8.3%. Although the PCE of the gas quenching-assisted slot-die-coated cells was relatively low, this was primarily linked to the need for further optimization of the coating process and the careful selection of precursor solutions to produce high-quality films [90].

Additive engineering strategies, such as Zuo et al.'s use of NH_4Cl in a blowing-assisted drop-casting method, also demonstrated feasibility for flexible substrates [91]. Mathilde and coworkers successfully revealed gas and heat-assisted crystallization of $\text{Cs}_{0.16}\text{FA}_{0.84}\text{Pb}(\text{I}_{0.88}\text{Br}_{0.12})_3$ perovskite using a slot-die coating process. This approach led to complete conversion to the cubic α -perovskite phase with compact, grain-like morphology on both TiO_2 and SnO_2 ETLs. The perovskite layers exhibited uniform thickness and coverage on $10 \times 10 \text{ cm}^2$ substrates. When incorporated into an (n-i-p) device configuration on SnO_2 -coated FTO substrates, these films achieved over 18% PCE on a 0.09 cm^2 active area, with a V_{OC} of 1024 mV. This represents the first report of scalable slot-die coated $\text{Cs}_y\text{FA}_{1-y}\text{Pb}(\text{I}_{1-x}\text{Br}_x)_3$ films with consistent thickness, controlled morphology, and crystallinity, without the use of chemical additives [49].

Li et al. investigated the influence of DMSO concentration in the 2-ME perovskite precursor solution, finding that a small addition of DMSO effectively inhibited the formation of undesirable intermediate phases. Consequently, they fabricated a slot-die-coated p-i-n solar cell device exhibiting an efficiency of 20.83%. For substrates measuring $2.5 \times 2.5 \text{ cm}^2$, with a total active device area of 2.2 cm^2 , the PCE statistics from 15 mini-modules yielded an average efficiency of 9.3% and a champion PCE of 14.6% [48].

Coating parameters for perovskite solution printing, specifically speed and gas velocity allow to predict the film drying dynamics. A quantitative drying model by incorporating key experimental parameters predicted heat transfer coefficients, calibrated with thermochromic and reflectometric measurements. This identifies that scaling success requires a heat transfer coefficient threshold of $500 \text{ W/m}^2 \text{ K}$ at the film's critical thickness, enabling a predictive 2D coating window validated through extensive testing. This model supports large-scale perovskite thin-film drying, offering critical parameters for optimized dryer systems and industrial production without interruption as shown in Figure 6b. There is a crucial relationship between the drying dynamics of slot-die coated precursor films and the quality of the resulting gas-quenched perovskite films. Using a temperature-controlled, movable table and a nitrogen-purged slot nozzle, Kristina et al. achieve precise film deposition and monitor the formation process in real-time with a CCD camera [26].

Duarte and co-workers found out that gas quenching is better adaptable for slot-die coating as compared to antisolvent because heating the perovskite layer and using an air knife to quench it externally produces uniform perovskite films. The substrate heating creates a temperature gradient that suppresses vertical crystal growth, promoting smoother, horizontal growth, resulting in better surface coverage. Additionally, they stated that this process was enhanced by combining blowing air with heating in a DMF solvent system. This approach accelerates nucleation and solvent evaporation, leading to void-free perovskite films and improved film quality [92].

Ke et al. also suggested that slot die coating combined with gas quenching for wide band gap perovskites gives reproducible results with it as shown in Figure 6c. They tried to reduce charge collection losses and enhanced current density by optimizing annealing parameters which in turn increases the grain sizes. Optimized results were

obtained at 150 °C [28].

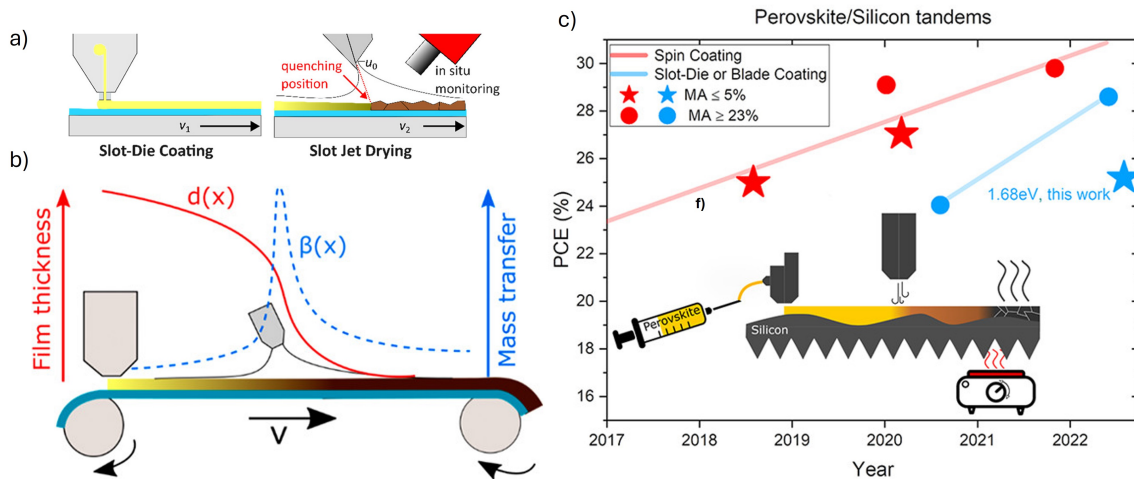


Figure 6. (a) Schematic representation of slot-die coating using gas quenching. Coating is applied at velocity v_1 , then nitrogen is introduced through a 50 μm slot jet at velocity v_2 . Reprinted with permission from [26]. Copyright 2023 American Chemical Society. (b) Quantitative model of the drying dynamics under oblique slot jets. Reprinted with permission from [27]. Copyright 2022 American Chemical Society. (c) Slot die coating for 1.68 eV wide bandgap perovskites. Reprinted with permission from [28]. Copyright 2022 American Chemical Society.

Slot-die coating offers several advantages, including high throughput, simple fabrication, and the ability to produce uniform films with precise control over thickness. It can create thin films with thicknesses as small as ≈ 20 nm. Additionally, it is well-suited for forming various layers in perovskite solar devices, such as ETLs, HTLs, perovskite layers, and carbon contacts, making it a versatile method for device fabrication. The other notable advantage it offers is that it gives better repeatable results. Whereas the shortcomings include its complexity, as multiple operational parameters must be optimized for effective performance. Additionally, the host solvent is not removed during the coating process, and film drying is carried out separately from the coating step. These factors can make the process more challenging to control and may require additional steps to achieve the desired film quality [93].

In summary, the advancements in gas-assisted coating methods have significantly improved the performance of large-area perovskite devices, paving the way for scalable efficient solar cell manufacturing.

7. Conclusions & Outlook

Gas quenching offers a highly repeatable and reproducible approach for the production of PSCs. Its tunable parameters provide significant flexibility in optimizing the preparation of the perovskite solution. This adaptability makes it compatible with additive strategies aimed at improving the stability and performance of perovskite absorber layers. In addition, gas quenching allows precise control over the crystallization and orientation of the perovskite layers. The benefits of gas quenching go beyond the limitations of a protected atmosphere. It can be used effectively in ambient conditions, as the gas used shields the surface from exposure to air.

While spin coating is effective for lab-scale PSC production, it is impractical for mass production. Scalable techniques such as blade coating and slot-die coating are better suited for commercialization because they minimize waste from precursor solution and are faster. However, problems such as uneven drying, non-uniformity, and sub-optimal solar cell performance currently hinder the large-area production of high-quality perovskite absorbers. To solve these problems, precise control of film deposition and crystallization is critical. While the antisolvent quenching is widely used, its scalability remains problematic, making the gas quenching an attractive alternative. Gas quenching allows control over perovskite crystallinity, orientation, drying speed, and uniformity, making it a viable strategy for improving film quality even in large-area processes.

Despite promising results and the successful demonstration of high-performing devices and modules, certain challenges related to gas quenching need to be further explored. For example, methylammonium-free films show poorer performance under gas quenching conditions. To address this issue, additive strategies have emerged as a common solution to help produce high-quality MA-free perovskite films. However, large-scale production with gas quenching has yet to achieve the same high efficiencies as spin-coated PSCs. Although larger cells or modules naturally suffer from efficiency losses due to extended charge extraction paths and increased series resistance, these are probably not the only factors.

While gas quenching offers elimination of antisolvents and flexibility to use greener solvents in perovskite precursor solutions, the energy usage and carbon emission due to compressed nitrogen production must be kept in mind. According to the European Industrial Gases Association (EIGA), the benchmark specific electricity consumption is 243 kWh per tonne of compressed nitrogen [94]. Also, the report from Tong et al. states that air separation process is responsible for approximately 2% of the CO₂ emission in USA and China [95]. Therefore, usage of nitrogen which is the most commonly used gas for gas quenching might hinder economical and environmental advantages that gas quenching has to offer.

To exploit the full potential of gas quenching in the production of large-area films, the mechanisms and the effects of the parameters on crystallization, grain size, and morphology need to be investigated in more detail. Using the flexibility of gas quenching to incorporate additives for crystallization control or passivation could be the key to achieving high-quality perovskite films and drive the commercialization of PSCs.

Given the advantages of gas quenching over the antisolvent method, we are confident that it will become increasingly important in the future and eventually replace antisolvent treatments. Therefore, it is crucial to investigate this promising technique in more detail in order to optimize the manufacturing processes and pave the way for large-scale production of PSCs and modules.

Funding

The authors of this paper are funded by DFG (Deutsche Forschungsgemeinschaft) and DAAD (deutscher akademischer Austauschdienst), research grant for doctoral programmes in Germany, funding number (57645448). D.T.C. gratefully acknowledges funding from the German Federal Ministry for Economic Affairs and Climate Action (BMWK) through the APERO project (ref. no. 03EE1113C).

Conflicts of Interest

The authors declare no conflict of interest.

References

1. NREL, Best Research-Cell Efficiencies. Available online: <https://www.nrel.gov/pv/cell-efficiency.html> (accessed on January 2025).
2. Kojima, A.; Teshima, K.; Shirai, Y.; et al. Organometal halide perovskites as visible-light sensitizers for photovoltaic cells. *J. Am. Chem. Soc.* **2009**, *131*, 6050–6051.
3. Feng, J.; Wang, X.; Li, J.; et al. Resonant perovskite solar cells with extended band edge. *Nat. Commun.* **2023**, *14*, 5392.
4. Temitmie, Y.A.; Haider, M.I.; Cuzzupè, D.T.; et al. Overcoming the Open-Circuit Voltage Losses in Narrow Bandgap Perovskites for All-Perovskite Tandem Solar Cells. *ACS Mater. Lett.* **2024**, *6*, 5190–5198.
5. Chiang, C.H.; Wu, C.G. Bulk heterojunction perovskite–PCBM solar cells with high fill factor. *Nat. Photonics* **2016**, *10*, 196–200.
6. Ergen, O.; Gilbert, S.M.; Pham, T.; et al. Graded bandgap perovskite solar cells. *Nat. Mater.* **2017**, *16*, 522–525.
7. Ouedraogo, N.A.N.; Chen, Y.; Xiao, Y.Y.; et al. Stability of all-inorganic perovskite solar cells. *Nano Energy* **2020**, *67*, 104249.
8. Qin, K.; Dong, B.; Wang, S. Improving the stability of metal halide perovskite solar cells from material to structure. *J. Energy Chem.* **2019**, *33*, 90–99.
9. Wang, K.; Zheng, L.; Zhu, T.; et al. Efficient perovskite solar cells by hybrid perovskites incorporated with heterovalent neodymium cations. *Nano Energy* **2019**, *61*, 352–360.
10. Zhang, W.; Eperon, G.E.; Snaith, H.J. Metal halide perovskites for energy applications. *Nature Energy* **2016**, *1*, 1–8.
11. Azhar, M.; Mubeen, M.; Mukhtar, M.; et al. Damping the phase segregation in mixed halide perovskites: Influence of X-site anion. *Mater. Chem. Phys.* **2022**, *287*, 126335.
12. Tavakoli, M.M.; Yadav, P.; Prochowicz, D.; et al. Controllable perovskite crystallization via antisolvent technique using chloride additives for highly efficient planar perovskite solar cells. *Adv. Energy Mater.* **2019**, *9*, 1803587.
13. Zhang, W.; Zhang, T.; Qin, L.; et al. Anti-solvent engineering to rapid purify PbI₂ for efficient perovskite solar cells. *Chem. Eng. J.* **2024**, *479*, 147838.
14. Zhao, P.; Kim, B.J.; Ren, X.; et al. Antisolvent with an ultrawide processing window for the one-step fabrication of efficient and large-area perovskite solar cells. *Adv. Mater.* **2018**, *30*, 1802763.
15. Jin, S.; Wei, Y.; Huang, F.; et al. Enhancing the perovskite solar cell performance by the treatment with mixed anti-solvent. *J. Power Sources* **2018**, *404*, 64–72.
16. Subhani, W.S.; Wang, K.; et al. Anti-solvent engineering for efficient semitransparent CH₃NH₃PbBr₃ perovskite solar cells for greenhouse applications. *J. Energy Chem.* **2019**, *34*, 12–19.

17. Taylor, A.D.; Sun, Q.; Goetz, K.P.; et al. A general approach to high-efficiency perovskite solar cells by any antisolvent. *Nat. Commun.* **2021**, *12*, 1878.
18. Paek, S.; Schouwink, P.; Athanasopoulou, E.N.; et al. From nano-to micrometer scale: The role of antisolvent treatment on high performance perovskite solar cells. *Chem. Mater.* **2017**, *29*, 3490–3498.
19. Ghosh, S.; Mishra, S.; Singh, T. Antisolvents in perovskite solar cells: Importance, issues, and alternatives. *Adv. Mater. Interfaces* **2020**, *7*, 2000950.
20. Cuzzupè, D.T.; Öz, S.D.; Ling, J.; et al. Understanding the Methylammonium Chloride-Assisted Crystallization for Improved Performance of Lead-Free Tin Perovskite Solar Cells. *Solar RRL* **2023**, *7*, 2300770.
21. Kaczaral, S.C.; Morales, D.A.; Schreiber, S.W.; et al. Improved reproducibility of metal halide perovskite solar cells via automated gas quenching. *APL Energy* **2023**, *1*, 036112.
22. Gou, Y.; Tang, S.; Yun, C.; et al. Research progress of green antisolvent for perovskite solar cells. *Mater. Horiz.* **2024**, *11*, 3465–3481.
23. Huang, F.; Dkhissi, Y.; Huang, W.; et al. Gas-assisted preparation of lead iodide perovskite films consisting of a monolayer of single crystalline grains for high efficiency planar solar cells. *Nano Energy* **2014**, *10*, 10–18.
24. Deng, Y.; Van Brackle, C.H.; Dai, X.; et al. Tailoring solvent coordination for high-speed, room-temperature blading of perovskite photovoltaic films. *Sci. Adv.* **2019**, *5*, eaax7537.
25. Subbiah, A.S.; Torres Merino, L.V.; Pininti, A.R.; et al. Enhancing the Performance of Blade-Coated Perovskite/Silicon Tandems via Molecular Doping and Interfacial Energy Alignment. *ACS Energy Lett.* **2024**, *9*, 727–731.
26. Geistert, K.; Ternes, S.; Ritzer, D.B.; et al. Controlling Thin Film Morphology Formation during Gas Quenching of Slot-Die Coated Perovskite Solar Modules. *ACS Appl. Mater. Interfaces* **2023**, *15*, 52519–52529.
27. Ternes, S.; Mohacsí, J.; Lüdtke, N.; et al. Drying and coating of perovskite thin films: How to control the thin film morphology in scalable dynamic coating systems. *ACS Appl. Mater. Interfaces* **2022**, *14*, 11300–11312.
28. Xu, K.; Al-Ashouri, A.; Peng, Z.W.; et al. Slot-die coated triple-halide perovskites for efficient and scalable perovskite/silicon tandem solar cells. *ACS Energy Lett.* **2022**, *7*, 3600–3611.
29. LaMer, V.K.; Dinegar, R.H. Theory, Production and Mechanism of Formation of Monodispersed Hydrosols. *J. Am. Chem. Soc.* **1950**, *72*, 4847–4854.
30. Qiu, S.; Majewski, M.; Dong, L.; et al. In Situ Probing the Crystallization Kinetics in Gas-Quenching-Assisted Coating of Perovskite Films. *Adv. Energy Mater.* **2024**, *14*, 2303210.
31. Liu, C.; Cheng, Y.B.; Ge, Z. Understanding of perovskite crystal growth and film formation in scalable deposition processes. *Chem. Soc. Rev.* **2020**, *49*, 1653–1687.
32. Wang, Z.; Duan, X.; Zhang, J.; et al. Manipulating the crystallization kinetics of halide perovskites for large-area solar modules. *Commun. Mater.* **2024**, *5*, 131.
33. Song, S.; Hörantner, M.T.; Choi, K.; et al. Inducing swift nucleation morphology control for efficient planar perovskite solar cells by hot-air quenching. *J. Mater. Chem. A* **2017**, *5*, 3812–3818.
34. Kim, M.; Kim, G.H.; Oh, K.S.; et al. High-temperature–short-time annealing process for high-performance large-area perovskite solar cells. *ACS Nano* **2017**, *11*, 6057–6064.
35. Zheng, D.; Raffin, F.; Volovitch, P.; et al. Control of perovskite film crystallization and growth direction to target homogeneous monolithic structures. *Nat. Commun.* **2022**, *13*, 6655.
36. Chen, S.; Xiao, X.; Chen, B.; et al. Crystallization in one-step solution deposition of perovskite films: Upward or downward? *Sci. Adv.* **2021**, *7*, eabb2412.
37. Xiao, M.; Huang, F.; Huang, W.; et al. A fast deposition-crystallization procedure for highly efficient lead iodide perovskite thin-film solar cells. *Angew. Chem. Int. Ed.* **2014**, *53*, 9898–9903.
38. Jeon, N.J.; Noh, J.H.; Kim, Y.C.; et al. Solvent engineering for high-performance inorganic–organic hybrid perovskite solar cells. *Nat. Mater.* **2014**, *13*, 897–903.
39. Lee, K.M.; Lin, C.J.; Liou, B.Y.; et al. Selection of anti-solvent and optimization of dropping volume for the preparation of large area sub-module perovskite solar cells. *Sol. Energy Mater. Sol. Cells* **2017**, *172*, 368–375.
40. Lin, K.F.; Chang, S.H.; Wang, K.H.; et al. Unraveling the high performance of tri-iodide perovskite absorber based photovoltaics with a non-polar solvent washing treatment. *Sol. Energy Mater. Sol. Cells* **2015**, *141*, 309–314.
41. Ahn, N.; Son, D.Y.; Jang, I.H.; et al. Highly reproducible perovskite solar cells with average efficiency of 18.3% and best efficiency of 19.7% fabricated via Lewis base adduct of lead (II) iodide. *J. Am. Chem. Soc.* **2015**, *137*, 8696–8699.
42. Lee, J.W.; Dai, Z.; Lee, C.; et al. Tuning molecular interactions for highly reproducible and efficient formamidinium perovskite solar cells via adduct approach. *J. Am. Chem. Soc.* **2018**, *140*, 6317–6324.
43. Cohen, B.E.; Aharon, S.; Dymshits, A.; et al. Impact of antisolvent treatment on carrier density in efficient hole-conductor-free perovskite-based solar cells. *J. Phys. Chem. C* **2016**, *120*, 142–147.
44. Etgar, L.; Gao, P.; Xue, Z.; et al. Mesoscopic CH₃NH₃PbI₃/TiO₂ heterojunction solar cells. *J. Am. Chem. Soc.* **2012**, *134*, 17396–17399.
45. Mei, A.; Li, X.; Liu, L.; et al. A hole-conductor-free, fully printable mesoscopic perovskite solar cell with high stability. *Science* **2014**, *345*, 295–298.

46. Ternes, S.; Laufer, F.; Paetzold, U.W. Modeling and Fundamental Dynamics of Vacuum, Gas, and Antisolvent Quenching for Scalable Perovskite Processes. *Adv. Sci.* **2024**, *11*, 2308901.
47. Wołowiec-Korecka, E. Development of Quenching Towards Quality Improvement. In *Carburising and Nitriding of Iron Alloys*; Springer: Berlin, Germany, 2024; pp. 71–85.
48. Yu, Y.; Zhang, F.; Hou, T.; et al. A Review on Gas-Quenching Technique for Efficient Perovskite Solar Cells. *Solar RRL* **2021**, *5*, 2100386.
49. Fievez, M.; Rana, P.J.S.; Koh, T.M.; et al. Slot-die coated methylammonium-free perovskite solar cells with 18% efficiency. *Sol. Energy Mater. Sol. Cells* **2021**, *230*, 111189.
50. Du, M.; Zhu, X.; Wang, L.; et al. High-pressure nitrogen-extraction and effective passivation to attain highest large-area perovskite solar module efficiency. *Adv. Mater.* **2020**, *32*, 2004979.
51. Hou, T.; Zhang, M.; Yu, W.; et al. Low-pressure accessible gas-quenching for absolute methylammonium-free perovskite solar cells. *J. Mater. Chem. A* **2022**, *10*, 2105–2112.
52. Conings, B.; Babayigit, A.; Klug, M.T.; et al. A universal deposition protocol for planar heterojunction solar cells with high efficiency based on hybrid lead halide perovskite families. *Adv. Materials.-Weinh.* **2016**, *28*, 10701–10709.
53. Babayigit, A.; D’Haen, J.; Boyen, H.G.; et al. Gas quenching for perovskite thin film deposition. *Joule* **2018**, *2*, 1205–1209.
54. Tang, S.; Bing, J.; Zheng, J.; et al. Complementary bulk and surface passivations for highly efficient perovskite solar cells by gas quenching. *Cell Rep. Phys. Sci.* **2021**, *2*, 100511.
55. Zhang, X.; Eurelings, S.; Brancesco, A.; et al. Surface Modulation via Conjugated Bithiophene Ammonium Salt for Efficient Inverted Perovskite Solar Cells. *ACS Appl. Mater. Interfaces* **2023**, *15*, 46803–46811.
56. Wu, Y.; Wu, S.; Wang, J.; et al. Facet orientation control of tin-lead perovskite for efficient all-perovskite tandem solar cells. *J. Mater. Sci. Technol.* **2025**, *213*, 118–124.
57. Heydarian, M.; Heydarian, M.; Bett, A.J.; et al. Monolithic Two-Terminal Perovskite/Perovskite/Silicon Triple-Junction Solar Cells with Open Circuit Voltage >2.8 V. *ACS Energy Lett.* **2023**, *8*, 4186–4192.
58. Brinkmann, K.O.; He, J.; Schubert, F.; et al. Extremely robust gas-quenching deposition of halide perovskites on top of hydrophobic hole transport materials for inverted (p–i–n) solar cells by targeting the precursor wetting issue. *ACS Appl. Mater. Interfaces* **2019**, *11*, 40172–40179.
59. Szostak, R.; Sanchez, S.; Marchezi, P.E.; et al. Revealing the perovskite film formation using the gas quenching method by in situ GIWAXS: Morphology, properties, and device performance. *Adv. Funct. Mater.* **2021**, *31*, 2007473.
60. Sun, X.; Yang, X.; Wang, X.; et al. The effect of pyrrolidone-based ligands in gas-quenching fabrication of FA0.9Cs0.1PbI3 perovskite films and solar cells. *J. Alloys Compd.* **2023**, *960*, 170670.
61. Harnmanasvate, C.; Chanajaree, R.; Rujisamphan, N.; et al. Ambient Gas-Quenching Fabrication of MA-Free Perovskite Solar Cells Enabled by an Eco-Friendly Urea Additive. *ACS Appl. Energy Mater.* **2023**, *6*, 10665–10673.
62. Werner, J.; Moot, T.; Gossett, T.A.; et al. Improving low-bandgap tin–lead perovskite solar cells via contact engineering and gas quench processing. *ACS Energy Lett.* **2020**, *5*, 1215–1223.
63. Zhang, X.; Qiu, W.; Aperi, S.; et al. Minimizing the Interface-Driven Losses in Inverted Perovskite Solar Cells and Modules. *ACS Energy Lett.* **2023**, *8*, 2532–2542.
64. Song, W.; Zhang, X.; Lammar, S.; et al. Critical Role of Perovskite Film Stoichiometry in Determining Solar Cell Operational Stability: A Study on the Effects of Volatile A-Cation Additives. *ACS Appl. Mater. Interfaces* **2022**, *14*, 27922–27931.
65. Öcbebe, A.; Deveci, H.; İsmail, C.K. Gas-Quenching Approach for Fabricating Cs₂ AgBiBr₆ Thin Films in Ambient Environment for Lead-Free All-Inorganic Perovskite Solar Cells with Carbon Electrodes. *Energy Technol.* **2023**, *11*, 2300407.
66. Öcbebe, A.; İsmail, C.K. From particles to films: Production of Cs₂ AgBiBr₆-based perovskite solar cells and enhancement of cell performance via ionic liquid utilization at the TiO₂/perovskite interface. *Dalton Trans.* **2024**, *53*, 1253–1264.
67. Zhang, M.; Yun, J.S.; Ma, Q.; et al. High-efficiency rubidium-incorporated perovskite solar cells by gas quenching. *ACS Energy Lett.* **2017**, *2*, 438–444.
68. Cassella, E.J.; Spooner, E.L.; Smith, J.A.; et al. Binary Solvent System Used to Fabricate Fully Annealing-Free Perovskite Solar Cells. *Adv. Energy Mater.* **2023**, *13*, 2203468.
69. Razza, S.; Di Giacomo, F.; Matteocci, F.; et al. Perovskite solar cells and large area modules (100 cm²) based on an air flow-assisted PbI₂ blade coating deposition process. *J. Power Sources* **2015**, *277*, 286–291.
70. Gao, L.L.; Li, C.X.; Li, C.J.; et al. Large-area high-efficiency perovskite solar cells based on perovskite films dried by the multi-flow air knife method in air. *J. Mater. Chem. A* **2017**, *5*, 1548–1557.
71. Gao, L.L.; Zhang, K.J.; Chen, N.; et al. Boundary layer tuning induced fast and high performance perovskite film precipitation by facile one-step solution engineering. *J. Mater. Chem. A* **2017**, *5*, 18120–18127.
72. Cheng, R.; Chung, C.C.; Zhang, H.; et al. An Air Knife-Assisted Recrystallization Method for Ambient-Process Planar Perovskite Solar Cells and Its Dim-Light Harvesting. *Small* **2019**, *15*, 1804465.
73. Lee, D.K.; Jeong, D.N.; Ahn, T.K.; et al. Precursor engineering for a large-area perovskite solar cell with >19% efficiency. *ACS Energy Lett.* **2019**, *4*, 2393–2401.

74. Dai, X.; Deng, Y.; Van Brackle, C.H.; et al. Scalable fabrication of efficient perovskite solar modules on flexible glass substrates. *Adv. Energy Mater.* **2020**, *10*, 1903108.
75. Chung, J.; Kim, S.; Li, Y.; et al. Engineering Perovskite Precursor Inks for Scalable Production of High-Efficiency Perovskite Photovoltaic Modules. *Adv. Energy Mater.* **2023**, *13*, 2300595.
76. Liang, Q.; Liu, K.; Sun, M.; et al. Manipulating Crystallization Kinetics in High-Performance Blade-Coated Perovskite Solar Cells via Cosolvent-Assisted Phase Transition. *Adv. Mater.* **2022**, *34*, 2200276.
77. Yue, W.; Yang, H.; Cai, H.; et al. Printable High-Efficiency and Stable FAPbBr₃ Perovskite Solar Cells for Multifunctional Building-Integrated Photovoltaics. *Adv. Mater.* **2023**, *35*, 2301548.
78. Jafarzadeh, F.; Castriotta, L.A.; Rossi, F.D.; et al. All-blade-coated flexible perovskite solar cells & modules processed in air from a sustainable dimethyl sulfoxide (DMSO)-based solvent system. *Sustain. Energy Fuels* **2023**, *7*, 2219–2228.
79. Pious, J.K.; Lai, H.; Hu, J.; et al. In Situ Buried Interface Engineering towards Printable Pb–Sn Perovskite Solar Cells. *ACS Appl. Mater. Interfaces* **2024**, *16*, 39399–39407.
80. Du, T.; Rehm, V.; Qiu, S.; et al. Precursor-Engineered Volatile Inks Enable Reliable Blade-Coating of Cesium–Formamidinium Perovskites Toward Fully Printed Solar Modules. *Adv. Sci.* **2024**, *11*, 2401783.
81. Hou, T.; Zhang, M.; Sun, X.; et al. Methylammonium-Free Ink for Low-Temperature Crystallization of α -FAPbI₃ Perovskite. *Adv. Energy Mater.* **2024**, *14*, 2400932.
82. Küffner, J.; Hanisch, J.; Wahl, T.; et al. One-Step Blade Coating of Inverted Double-Cation Perovskite Solar Cells from a Green Precursor Solvent. *ACS Appl. Energy Mater.* **2021**, *4*, 11700–11710.
83. Fong, P.W.; Hu, H.; Ren, Z.; et al. Printing High-Efficiency Perovskite Solar Cells in High-Humidity Ambient Environment—An In Situ Guided Investigation. *Adv. Sci.* **2021**, *8*, 2003359.
84. Vesce, L.; Stefanelli, M.; Herterich, J.P.; et al. Ambient Air Blade-Coating Fabrication of Stable Triple-Cation Perovskite Solar Modules by Green Solvent Quenching. *Solar RRL* **2021**, *5*, 2100073.
85. Vesce, L.; Stefanelli, M.; Rossi, F.; et al. Perovskite solar cell technology scaling-up: Eco-efficient and industrially compatible sub-module manufacturing by fully ambient air slot-die/blade meniscus coating. *Prog. Photovolt. Res. Appl.* **2024**, *32*, 115–129.
86. Ding, J.; Han, Q.; Ge, Q.Q.; et al. Fully air-bladed high-efficiency perovskite photovoltaics. *Joule* **2019**, *3*, 402–416.
87. Kistler, S.; Scriven, L. Coating flows. In *Computational Analysis of Polymer Processing*; Springer: Berlin, Germany, 1983; pp. 243–299.
88. Cotella, G.; Baker, J.; Worsley, D.; et al. One-step deposition by slot-die coating of mixed lead halide perovskite for photovoltaic applications. *Sol. Energy Mater. Sol. Cells* **2017**, *159*, 362–369.
89. Kim, J.E.; Jung, Y.S.; Heo, Y.J.; et al. Slot die coated planar perovskite solar cells via blowing and heating assisted one step deposition. *Sol. Energy Mater. Sol. Cells* **2018**, *179*, 80–86.
90. Lee, D.; Jung, Y.S.; Heo, Y.J.; et al. Slot-die coated perovskite films using mixed lead precursors for highly reproducible and large-area solar cells. *ACS Appl. Mater. Interfaces* **2018**, *10*, 16133–16139.
91. Zuo, C.; Vak, D.; Angmo, D.; et al. One-step roll-to-roll air processed high efficiency perovskite solar cells. *Nano Energy* **2018**, *46*, 185–192.
92. Duarte, V.C.; Andrade, L. Recent Advancements on Slot-Die Coating of Perovskite Solar Cells: The Lab-to-Fab Optimisation Process. *Energies* **2024**, *17*, 3896.
93. Matondo, J.T.; Hu, H.; Ding, Y.; et al. Slot-Die Coating for Scalable Fabrication of Perovskite Solar Cells and Modules. *Adv. Mater. Technol.* **2024**, *9*, 2302082.
94. Indirect CO₂ Emissions Compensation: Benchmark Proposal for Air Separation Plants. Available online: <https://www.eiga.eu/uploads/documents/PP033.pdf> (accessed on February 2025).
95. Tong, L.; Zhang, A.; Li, Y.; et al. Exergy and energy analysis of a load regulation method of CVO of air separation unit. *Appl. Therm. Eng.* **2015**, *80*, 413–423.